

Mechanistic inference of the metabolic rates underlying ^{13}C breath test curves

Andrew F. Brouwer (✉ brouweaf@umich.edu)

University of Michigan

Gwenyth O. Lee

University of Michigan

Robert J. Schillinger

University of Glasgow

Christine A. Edwards

University of Glasgow

Hannah Van Wyk

University of Michigan

Roger Yazbeck

Flinders University

Douglas J. Morrison

Scottish Universities Environmental Research Centre

Research Article

Keywords: carbon-13, stable isotope, breath test, sucrose, identifiability, environmental enteric dysfunction

Posted Date: September 19th, 2022

DOI: <https://doi.org/10.21203/rs.3.rs-2070340/v1>

License:  This work is licensed under a Creative Commons Attribution 4.0 International License.

[Read Full License](#)

Mechanistic inference of the metabolic rates underlying ^{13}C breath test curves

Andrew F. Brouwer (0000-0002-3779-5287)^{1*}, Gwenyth O. Lee ((0000-0002-7889-3852))¹, Robert J. Schillinger^{2,3}, Christine A. Edwards (0000-0003-0406-918X)³, Hannah Van Wyk (0000-0002-3495-0085)¹, Roger Yazbeck⁴ and Douglas J. Morrison (0000-0002-4161-5699)²

¹*Department of Epidemiology, University of Michigan, 1415 Washington Heights, Ann Arbor, 48109, MI, United States.

²Scottish Universities Environmental Research Centre, University of Glasgow, Rankine Avenue, East Kilbride, G75 0QF, United Kingdom.

³School of Medicine, Dentistry and Nursing, University of Glasgow, University Ave, Glasgow, G12 8QQ, United Kingdom.

³College of Medicine and Public Health, Flinders University, University Ave, Adelaide, 5001, South Australia.

*Corresponding author(s). E-mail(s): brouweaf@umich.edu; +1 773-764-7373;

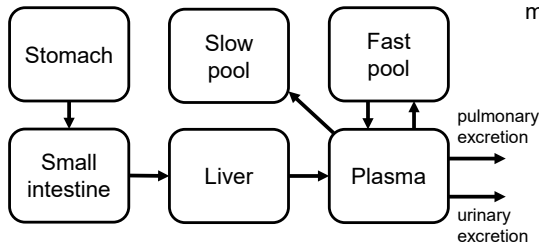
Abstract

Carbon stable isotope breath tests offer new opportunities to better understand gastrointestinal function in health and disease. However, it is often not clear how to isolate information about a gastrointestinal or metabolic process of interest from a breath test curve, and it is generally unknown how well summary statistics from empirical curve fitting correlate with underlying biological rates. We developed a framework that can be used to make mechanistic inference about the metabolic rates underlying a ^{13}C breath test curve, and we applied it to a pilot study of ^{13}C -sucrose breath test in 20 healthy adults. Starting from a standard conceptual model of sucrose metabolism, we determined the structural and practical identifiability of the model, using algebra and profile likelihoods, respectively, and we used these results

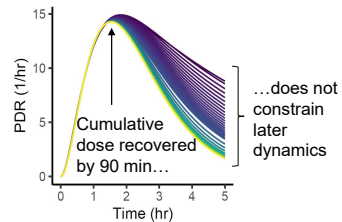
2 *Mechanistic inference for ¹³C breath test curves*

to develop a reduced, identifiable model as a function of a gamma-distributed process, a slower, rate-limiting process, and a scaling term related to the fraction of the substrate that is exhaled as opposed to sequestered or excreted through urine. We demonstrated how the identifiable model parameters impacted curve dynamics and how these parameters correlated with commonly used breath test summary measures. Our work develops a better understanding of how the underlying biological processes impact different aspects of ¹³C breath test curves, enhancing the clinical and research potential of these ¹³C breath tests.

Keywords: carbon-13, stable isotope, breath test, sucrose, identifiability, environmental enteric dysfunction

Tracer metabolism in a ¹³C breath test

Standard summary measures may not adequately inform underlying metabolism



Introduction

Carbon stable isotope breath tests offer new opportunities to better understand gastrointestinal function in health and disease [1]. These tests provide a dose of non-radioactive ¹³C-labeled substrate, which is digested, absorbed and metabolized, appearing on the breath as ¹³CO₂. As the range of labeled substrates that are commercially available grows, from whole-molecule labeling to position-specific (atom-level) labeling, ¹³C breath tests can be developed to target a wide range of specific gut processes, such as digestion, absorption, or oxidation, with a correspondingly wide range of potential clinical applications.

Beyond one or two clinical tests with clear diagnostic criteria, the uses of ¹³C breath tests have remained primarily limited to research, in part because standard methods to characterize ¹³C breath test curves often reflect a complicated mix of both the underlying biological process of interest and other aspects of metabolism. For this reason, the most successful ¹³C breath tests have relatively simple dynamics—such as the ¹³C urea breath for detection of *Helicobacter pylori*—or are carefully designed to ensure that the biological process of interest is the rate-limiting process. For example, the ¹³C-octanoic acid

breath test is based on the fact that medium-chain fatty acids are absorbed immediately on entering the duodenum, which causes gastric emptying to be the rate-limiting step [2]. In the ¹³C-galactose test of hepatic function, the rate-limiting step is the hepatic clearance of galactose [3].

However, in other cases, it is not clear how to isolate information about a gastrointestinal or metabolic process of interest from a breath test curve (serial measurements of ¹³CO₂ concentration in the breath over time). Breath test curves can be characterized by empirical curve fitting and by summary measures, often themselves derived from curve fitting results. However, these metrics do not necessarily correspond directly to biological processes. Curve fitting models of the percent dose recovery rate (PDR), here denoted $y(t)$, include an empirical gamma function [4]

$$y(t) = at^b \exp(-ct), \quad (1)$$

and the following function derived from an empirical assumption about gastric emptying [5, 6],

$$y(t) = \frac{d}{dt} m [1 - \exp(-kt)]^\beta = mk\beta \exp(-kt) [1 - \exp(-kt)]^{\beta-1}. \quad (2)$$

These methods can be applied to ¹³C breath test curves, often with reasonable fits. However, the success of an empirical model only indicates that it is sufficiently flexible to capture features of the curve, not that it can offer mechanistic insight. Moreover, while many breath test curve summary measures have been proposed, e.g., cumulative percent dosed recovered (cPDR) by time t , peak PDR, time to peak PDR, and time to recover 50% of the dose (cPDR-50), their connection to specific processes of interest is weak. Nevertheless, certain summary measures are typically preferable to others for certain inferences, suggesting that there is some mechanistic connection between the biological rates and the dynamics captured by the summary measures. For instance, the time to peak PDR has been shown to out-perform the time to recovery of 50% of the dose for gastric emptying [7].

In this analysis, we return to pharmacokinetic modeling fundamentals to develop a framework that can be used to make mechanistic inference about the metabolic rates underlying a ¹³C breath test curve. We also demonstrate how these mechanistic parameters isolate aspects of breath test curve dynamics and how they correlate with standard curve summary measures. We illustrate this framework using ¹³C sucrose breath test (¹³C-SBT) curves from 20 healthy volunteers. The ¹³C-SBT has been proposed as a measure of intestinal brush-border sucrase function to assess environmental enteric dysfunction (EED) [8]. EED is a syndrome characterized by villous atrophy (also called villous blunting), inflammation, and increased permeability of the small intestine [9, 10] and is thought to be ubiquitous among the 2 billion children and adults who lack access to improved water or sanitation in low- and middle-income countries [11]. Prior studies have suggested that sucrase activity is disrupted in

EED [12], as well as in celiac disease (CD) and other gastrointestinal disorders with functional similarities to EED [13–16]. Accordingly, understanding how ¹³C-SBT curves reflect healthy or disrupted sucrase activity may have important clinical and global public health applications, making it an appropriate motivating example for this theoretical work.

Methods

Data

Twenty health adults were recruited to participate in a proof-of-concept ¹³C-SBT study. Participants were recruited by advertisement in the Glasgow area, aged between 18–65 years with no history of gastrointestinal symptoms or disease. The cohort mean (standard deviation) BMI was 22.0 (3.5) kg/m², mean age was 22.8 (4.6) years and male-to-female ratio was 10/10. Participants gave informed consent, and the study was approved by the University of Glasgow College of Medical, Veterinary & Life Sciences Research Ethics Committee (Application Number: 200170060). Because the biological process of interest in this test is intestinal sucrase activity, the tracer was given as a small, liquid dose (50mg ¹³C-sucrose in 100ml water) to minimize delay from gastric emptying.

Isotope abundance in the samples was measured as $\delta^{13}\text{C}$, the relative difference in parts per thousand between the sample and the internationally accepted calibration standard ratio ($R=0.0112372$) of ¹³C/¹²C [17]. This measure was converted to ppm ¹³C,

$$\text{ppm } ^{13}\text{C} = \frac{10^6}{1 + \frac{1}{\left(\frac{\delta^{13}\text{C}}{1,000} + 1\right) \cdot R}}. \quad (3)$$

Excess ppm ¹³C over baseline was converted to percent dose recovered (PDR) per hour,

$$\text{PDR}(t) = \frac{100 \cdot (\text{ppm } ^{13}\text{C at time } t - \text{ppm } ^{13}\text{C at time } 0) \cdot V_{\text{CO}_2}}{10^6 \cdot \text{dose of } ^{13}\text{C (mmol)}}, \quad (4)$$

where V_{CO_2} is a subject-specific estimate of CO₂ production (mmol/hour) based on the participant’s estimated body surface area and sex [18].

Mathematical model

We use a standard conceptual model of carbon substrate (here, sucrose) metabolism as a starting point for a compartmental, ordinary differential equation model of a ¹³C substrate breath test. In this conceptual model (**Figure 1a**), the ingested tracer enters the stomach and passes to the small intestine (gastric emptying). For the motivating example, sucrase-isomaltase secreted in the brush-border at the villous tips cleaves sucrose into glucose

and fructose, facilitating active transport for glucose and fructose moieties into the blood, where the substrate moves to the liver via the hepatic portal. The substrates are oxidized in the liver through a series of intermediary metabolic processes and converted to bicarbonate. Bicarbonate kinetics are typically modeled with a fast pool and a slow pool [19]. Transfer to the slow pool, representing long-term processes such as lipid storage, is often considered to be irreversible on the time scale of a breath test. Plasma bicarbonate has two excretion pathways, urinary and pulmonary. Through the ¹³C breath test, pulmonary excretion of ¹³CO₂ is observed.

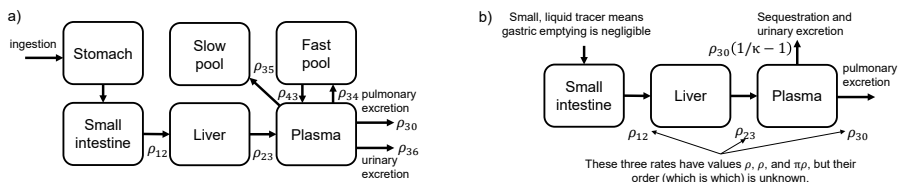


Fig. 1 a). A conceptual model of carbon breath test kinetics includes physical transport, metabolism, bicarbonate kinetics, and excretion. b) A structurally and practically identifiable model of carbon breath test kinetics.

Given the nature of the liquid sucrose tracer and the physiology of the stomach, we model the residence time in the stomach as a time-delay (although no time delay was needed for these participants) and all other processes as mass action. The fraction of the ¹³C dose in each of the small intestine, liver, plasma bicarbonate, fast bicarbonate pool, and slow bicarbonate pool are denoted by x_1 through x_5 , respectively. Let ρ_{ij} be the rate of transfer from compartment x_i to x_j . Let ρ_{30} be the pulmonary excretion and ρ_{36} the urinary excretion rates of bicarbonate from plasma. Then, the ordinary differential equations are as follows.

$$\begin{aligned}
 \frac{dx_1}{dt} &= -\rho_{12}x_1, \\
 \frac{dx_2}{dt} &= \rho_{12}x_1 - \rho_{23}x_2, \\
 \frac{dx_3}{dt} &= \rho_{23}x_2 - (\rho_{30} + \rho_{34} + \rho_{35} + \rho_{36})x_3 + \rho_{43}x_4, \\
 \frac{dx_4}{dt} &= \rho_{34}x_3 - \rho_{43}x_4, \\
 \frac{dx_5}{dt} &= \rho_{35}x_3.
 \end{aligned} \tag{5}$$

The initial conditions of this model are $x_1(0) = 100$ and all other $x_{i \neq 1}(0) = 0$. Through the breath test, we have the following measurement equation for PDR at time t ,

$$y(t) = \rho_{30}x_3(t) \tag{6}$$

We denote the full parameter set as $\boldsymbol{\theta}$. When we want to emphasize the dependence of the output on the parameters, we will write $y(\boldsymbol{\theta}, t)$.

Identifiability and model reduction

In the context of determining the health of the small intestine and ultimately diagnosing EED, the aim of the ¹³C-SBT is to infer the value of ρ_{12} , the rate of metabolism in the small intestine, given $y(t)$. But, before estimating the value of a model parameter from observed data, we first need to determine whether that parameter is *identifiable*, that is, whether there is a unique value of the parameter associated with the best fit of the proposed mechanistic model to the available data. If a parameter is not identifiable, i.e., multiple values or a range of values of the parameter can explain the data equally well, then we can find a simpler, reduced model that similarly fits the data but whose parameters are all identifiable. For example, if our model was $y = (m_1 + m_2)x + b$ for some (x, y) -pair data, parameter b would be identifiable, but parameters m_1 and m_2 would not be. However, we could reduce our model by defining a new parameter $m := m_1 + m_2$. Unfortunately, identifiability and model reduction are not so straightforward for even modestly complex differential equation models.

We distinguish between *structural identifiability*, which asks whether a parameter can be determined given perfect measurement of the model output [20–22], and *practical identifiability*, which asks whether a parameter can be measured given actual data [23]. A parameter may be structurally but not practically identifiable because of excessive noise, insufficiently regular measurement, or other reasons. Structural identifiability analysis is often a useful first step because it can determine identifiable parameter combinations, whose values are identifiable even if the constituent parameters are not individually identifiable and which may aid in model reduction. After structural identifiability is determined, practical identifiability analysis determines the real-world identifiability and uncertainty in parameter estimates given a level of significance (e.g., 95% confidence). If practical identifiability determines systematic lack of identifiability because of the nature of data collection (e.g., inability to observe certain characteristics of an output trajectory due to the time scales [24]), further model reduction is possible.

To determine the structural identifiability of our model parameters when observing $y(t)$, we first found an input–output equation of the model [25–27]. An input–output equation is a monic polynomial equation in terms of the measured input and output variables and their derivatives. The coefficients of an input–output equation represent the identifiable parameter combinations of the model for the given measurement. We used Wolfram Mathematica v11.3 (Wolfram Research; Champaign, Illinois) to determine an input–output equation for the model and measurement in Eqs (5) and (6).

To determine practical identifiability, we used profile likelihoods to determine how dependent the model fit to the data was on the specific values of the parameters. Profile likelihoods, which can be used to determine likelihood-based confidence intervals, vary the fixed value of one parameter while

determining the best fit (minimum negative log-likelihood) when fitting the remaining parameters [23, 24, 28]. If the likelihood-based confidence interval for a parameter has infinite width (for a given level of significance), then the parameter is not practically identifiable. Here, we used a normal log-likelihood as function of the parameters θ .

$$\log(\mathcal{L}(\theta)) = -\frac{n}{2} \log(2\pi) - \frac{n}{2} \log(\sigma^2) - \frac{1}{2\sigma^2} \sum_i (y(\theta, t_i) - z_i)^2 \quad (7)$$

where n is the number of data points and t_i is the time at which measurement z_i was taken. The variance σ^2 is estimated as $\frac{1}{n-1} \sum_i (y(\theta, t_i) - z_i)^2$ and thus depends on θ . Denote the maximum-likelihood estimate as $\hat{\theta}$. Denote the maximum likelihood when the i th parameter is fixed to value θ_i as $\mathcal{L}(\hat{\theta}_{j \neq i}, \theta_i)$ and call it the *profile likelihood* of θ_i . The likelihood based confidence interval at level of significance α is $\{\theta_i : \log(L(\hat{\theta})) - \log(L(\hat{\theta}_{j \neq i}, \theta_i)) < \Delta_\alpha\}$, where Δ_α is $\chi^2(\alpha, \text{df})/2$ where $\chi^2(\alpha, \text{df})$ is the chi-squared distribution with a number of degrees of freedom equal to the number of parameters and α is the level of significance [23]. In layman's terms, the profile likelihood tracks how much worse the "best" fit of the model to the data is as we constrain one parameter away from its maximum-likelihood estimate, and the level of significance determines the level of "how much worse of a fit" corresponds to the bounds of our confidence interval for θ_i .

We made simplifying assumptions based on the profile likelihoods to arrive at a series of reduced models. For parameters that are structurally identifiable but not practically identifiable, the choices of simplifying assumptions may be partially subjective, with multiple potential reductions. We explain our specific assumptions and justifications in the Results.

After arriving at a reduced, practically identifiable model, we compared fits of the original model and each of the reduced models to each of the 20 breath test curves. We analyzed our final, reduced model by comparing the dynamics of the simulated breath curves as a function of each of the reduced model parameters in turn. We also calculated the correlations of the values of the reduced model parameters fit to each of the 20 breath tests with each of four breath test curve summary measures (cPDR at 90 min, peak PDR, time to peak PDR, and time to cPDR-50) to assess how well these summary measures reflect the underlying mechanistic parameters. Model simulations and optimization were performed in R v4.0 (R Foundation for Statistical Computing; Vienna, Austria).

Results

Structural identifiability

We algebraically solve for an input–output equation for the model in Eq. 5 and the measurement model in Eq. 6,

$$\begin{aligned}
 0 = & \frac{d^4 y}{dt^4} + (\rho_{12} + \rho_{23} + \rho_{30} + \rho_{34} + \rho_{35} + \rho_{36} + \rho_{43}) \frac{d^3 y}{dt^3} \\
 & + (\rho_{12}\rho_{23} + \rho_{12}\rho_{30} + \rho_{12}\rho_{34} + \rho_{12}\rho_{35} + \rho_{12}\rho_{36} + \rho_{12}\rho_{43} \\
 & + \rho_{23}\rho_{30} + \rho_{23}\rho_{34} + \rho_{23}\rho_{35} + \rho_{23}\rho_{36} + \rho_{23}\rho_{43} + \rho_{30}\rho_{43} + \rho_{35}\rho_{43} + \rho_{36}\rho_{43}) \frac{d^2 y}{dt^2} \\
 & + (\rho_{12}\rho_{23}\rho_{30} + \rho_{12}\rho_{23}\rho_{34} + \rho_{12}\rho_{23}\rho_{35} + \rho_{12}\rho_{23}\rho_{36} + \rho_{12}\rho_{23}\rho_{43} \\
 & + \rho_{12}\rho_{30}\rho_{43} + \rho_{23}\rho_{30}\rho_{43} + \rho_{12}\rho_{35}\rho_{43} + \rho_{23}\rho_{35}\rho_{43} + \rho_{12}\rho_{36}\rho_{43} + \rho_{23}\rho_{36}\rho_{43}) \frac{dy}{dt} \\
 & + (\rho_{12}\rho_{23}\rho_{30}\rho_{43} + \rho_{12}\rho_{23}\rho_{35}\rho_{43} + \rho_{12}\rho_{23}\rho_{36}\rho_{43})y.
 \end{aligned} \tag{8}$$

This equation has four coefficients, which are four identifiable parameter combinations as a function of six parameters, meaning that the six parameters cannot be individually, uniquely determined by observing $y(t)$. Toward the goal of understanding and simplifying these parameters combinations, we introduce two reparameterized parameters, $\alpha = \rho_{30} + \rho_{34} + \rho_{35} + \rho_{36} + \rho_{43}$ and $\beta = \rho_{43}(\rho_{35} + \rho_{30} + \rho_{36})$. These reparameterizations simplify the input–output equation,

$$\begin{aligned}
 0 = & \frac{d^4 y}{dt^4} + (\rho_{12} + \rho_{23} + \alpha) \frac{d^3 y}{dt^3} \\
 & + (\beta + \rho_{12}\rho_{23} + \alpha(\rho_{12} + \rho_{23})) \frac{d^2 y}{dt^2} \\
 & + (\alpha\rho_{12}\rho_{23} + \beta(\rho_{12} + \rho_{23})) \frac{dy}{dt} \\
 & + (\beta\rho_{12}\rho_{23})y.
 \end{aligned} \tag{9}$$

The map from the four parameters $\{\alpha, \beta, \rho_{12}, \rho_{23}\}$ to the four coefficients of this input–output equation is not one-to-one, but there are only finitely many solutions. Hence, these parameter combinations are locally identifiable.

We also have information from the initial conditions of $y(t)$ and its derivatives. The initial conditions of y and $\frac{dy}{dt}$ are 0, but the initial condition of $\frac{d^2 y}{dt^2}$ is $\rho_{12}\rho_{23}\rho_{30}$ and the initial condition of $\frac{d^3 y}{dt^3}$ is $-\rho_{12}\rho_{23}\rho_{30}(\alpha + \rho_{12} + \rho_{23} - \rho_{43})$. Altogether, a minimal set of locally identifiable parameter combinations is then $\{\rho_{12}, \rho_{23}, \rho_{30}, \rho_{35} + \rho_{36}, \rho_{34}, \rho_{43}\}$. Parameters ρ_{12} , ρ_{23} , ρ_{30} , ρ_{34} , and ρ_{43} retain their original interpretations, but, because the parameters are only locally and not globally identifiable, we do not necessarily know which rate value belongs to which biological process. Parameter combination $\rho_{3-} := \rho_{30} + \rho_{35}$ is the

rate of the tracer leaving the body through urine or being sequestered in a bicarbonate pool. This last combination represents the fact that we cannot distinguish between tracer that has been sequestered in the slow bicarbonate pool and tracer that has been excreted in urine if we measure only pulmonary excretion. A structurally identifiable version of (5) is thus as follows.

$$\begin{aligned}
 \frac{dx_1}{dt} &= -\rho_{12}x_1, \\
 \frac{dx_2}{dt} &= \rho_{12}x_1 - \rho_{23}x_2, \\
 \frac{dx_3}{dt} &= \rho_{23}x_2 - (\rho_{34} + \rho_{30} + \rho_{3-})x_3 + \rho_{43}x_4, \\
 \frac{dx_4}{dt} &= \rho_{34}x_3 - \rho_{43}x_4, \\
 y(t) &= \rho_{30}x_3(t).
 \end{aligned} \tag{10}$$

The two take-aways from the structural identifiability analysis are that the slow bicarbonate pool is indistinguishable from urinary excretion and that even if we determine the values of the underlying biological rates, we cannot determine their order (e.g., we will not know which of the biological processes corresponds to the slowest, limiting rate).

Practical identifiability

Even if the above set of parameters and parameters combinations are structurally identifiable, they may not be practically identifiable from real-world breath test curves. To illustrate the practical identifiability of the model, we use data from the ¹³C-SBT and determine the profile likelihoods of each of the structurally identifiable parameters. Each set of data, along with the corresponding best fit by the full, structurally identifiable model (Eq (10)), are shown in Fig. 2. This plot also includes fits from a series of reduced models developed below.

In Fig. S1, we demonstrate that all parameters in the full structurally identifiable model are practically unidentifiable given real data, with the possible exception of ρ_{12} and ρ_{23} . Moreover, none of the relationships with the other parameters along these profiles are indicative of practically identifiable parameter combinations, e.g., no two parameters vary together in a way that suggests that their sum or product is constant. However, we do see that parameter ρ_{43} can be sent to 0 or ∞ with negligible loss of fit, suggesting that the dynamics of the fast bicarbonate kinetics do not meaningfully impact the breath test trajectory. For simplicity, we reduce our model by assuming $\rho_{43} = \rho_{34} = 0$. Finally, we define $\kappa := \rho_{30}/(\rho_{30} + \rho_{3-})$ to be the fraction of bicarbonate that is exhaled on the breath; this parameterization is convenient because it demonstrates that although ρ_{30} and ρ_{3-} can take multiple values depending on ρ_{12}

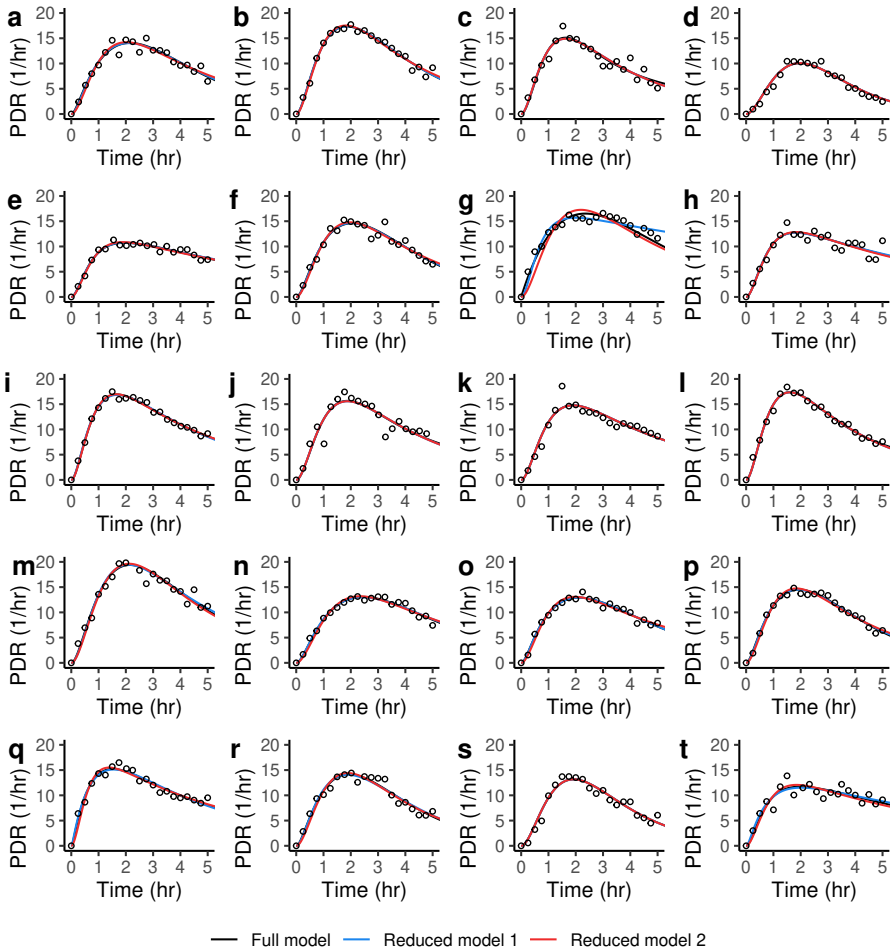


Fig. 2 ¹³C sucrose breath test trajectories for 20 adults, with fits from the full structurally identifiable model (Eq (10)) and reduced models (Eq (11)). With only a few exceptions, the reduced models are indistinguishable from the full model.

and ρ_{23} , there is a fixed relationship between them.

$$\begin{aligned}
 \frac{dx_1}{dt} &= -\rho_{12}x_1, \\
 \frac{dx_2}{dt} &= \rho_{12}x_1 - \rho_{23}x_2, \\
 \frac{dx_3}{dt} &= \rho_{23}x_2 - \rho_{30}x_3/\kappa, \\
 y(t) &= \rho_{30}x_3(t).
 \end{aligned}
 \tag{11}$$

The fit to each individual's breath test trajectory are shown in Figure 2 (Reduced model 1). The fits from Reduced model 1 reproduce the Full model fits in nearly all cases, confirming that the dynamics of the fast bicarbonate pool can be neglected.

We next compute the profile likelihoods for the four parameters in the model in Eq. (11) in Fig S2. Parameter κ is identifiable, which is sensible since it describes the asymptote of the cPDR. However, we find that ρ_{12} , ρ_{23} , and ρ_{30}/κ , which we know are only locally identifiable, are indeed interchangeable, so that they take 3 (possibly repeated) values between them. Only two local minima are observed for the three parameters for many plots, indicating that the likelihood wells for two of the rates have merged. Although for each individual's breath trajectory the likelihood profiles may prefer the two larger or two smaller values to be repeated (share the same value), we find that it is sufficient and more convenient to constrain the model so that the larger value is repeated. Thus, in our final model reduction in Eq (12), without loss of generality, we assume that the first step is the slowest, i.e., we set $\rho = \rho_{23} = \rho_{30}/\kappa$ and $\pi\rho = \rho_{12}$ where $\pi \leq 1$. Here, π defines how much smaller the lower rate is than the higher rates. It is important to note again that, because the parameters are only locally identifiable, we cannot determine which rate corresponds to which biological process. That is, we cannot determine which process has the limiting rate. In this reduced model,

$$\begin{aligned}\frac{dx_1}{dt} &= -\pi\rho x_1, \\ \frac{dx_2}{dt} &= \pi\rho x_1 - \rho x_2, \\ \frac{dx_3}{dt} &= \rho x_2 - \rho x_3, \\ y(t) &= \kappa\rho x_3(t).\end{aligned}\tag{12}$$

The fit to each individual's breath test trajectory are shown in Figure 2 (Reduced model 2), and the confirmation that the parameters are identifiable is given in Fig S3. The fits from Reduced model 2 reproduce the Full model fits in nearly all cases. This model also has a closed form solution. When $\pi < 1$,

$$y(t) = \frac{100\kappa\pi\rho}{(\pi - 1)^2} (\exp(-\pi\rho t) + ((\pi - 1)\rho t - 1) \exp(-\rho t))\tag{13}$$

The formula for the cumulative percent dose recovered is which has a horizontal asymptote of 100κ as $t \rightarrow \infty$.

Practically, this reduced model indicates that a single breath test curve can be summarized as resulting from a faster, gamma-distributed process and a slower, exponential process (in some order, possibly with the slower, exponential process occurring in-between portions of the other process). The fraction of the tracer that will be exhaled as opposed to sequestered or otherwise excreted scales the overall PDR. This final, reduced model is summarized in Figure 1b.

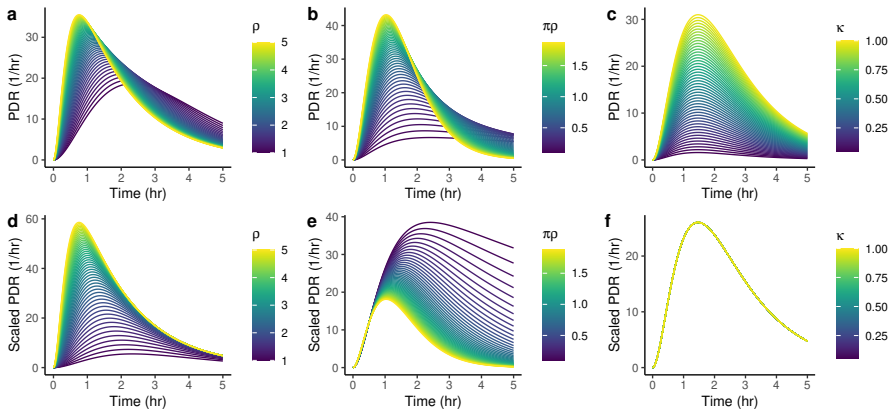


Fig. 3 (a–c) Breath test curve simulations setting ρ , $\pi\rho$, and κ to their mean values and then varying one parameter at a time, respectively. (d–f) Scaled versions of the simulations in (a–c), see text.

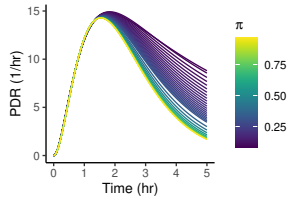


Fig. 4 Breath test curve simulations demonstrating that the dynamics of the early portion of the curve do not constrain the later curve. Here ρ and κ are chosen for each value of $\pi\rho$ in a way that preserves the dynamics up to 90 minutes.

Model dynamics

To understand how each of the 3 parameters ρ , $\pi\rho$, and κ impact the dynamics of the breath curve, we first take the mean values of each parameter across the 20 trajectories ($\bar{\rho}=1.97$, $\bar{\pi\rho}=0.32$, $\bar{\kappa}=0.82$). Then we vary one parameter while keeping the other two constant. The range of dynamics is shown in Fig 3a–c. In Fig 3d–f, we scale the curves in Fig 3a–c appropriately (by $(\bar{\pi\rho}(\bar{\pi}-1)^2)/(\pi\rho(\bar{\pi}-1)^2)$ in (a), by $\bar{\pi}/\pi$ in (b), and by $\bar{\kappa}/\kappa$ in (c)). The scaled figures highlight that ρ impacts the rate of increase, $\pi\rho$ controls the rate of decline, and κ is a vertical scaling factor.

These curves further suggest that the early part of the curve may not be informative for $\pi\rho$. Indeed, in Figure 4, we see that we can choose values of ρ and κ such that the early part of the curve (first 90 minutes) does not constrain the later part of the curve. This result suggests that certain summary measures may not be informative for certain underlying processes.

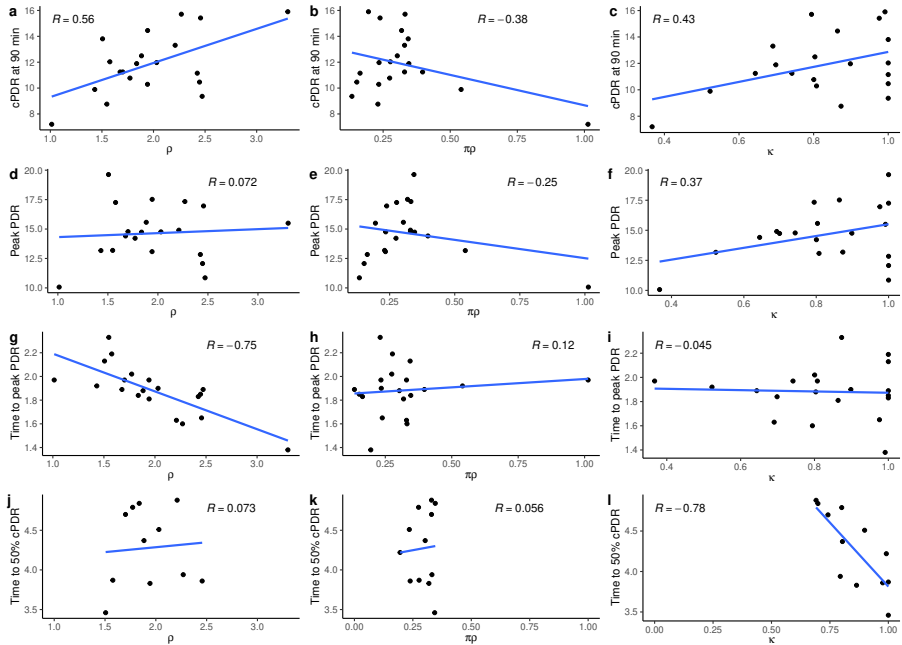


Fig. 5 Correlations between mechanistic model parameters estimated from 20 breath test curves and the corresponding summary measures of those curves.

Summary measures

Here, we compare the model parameters ρ , $\pi\rho$, and κ estimated for each of the 20 breath test curves to the estimated values of each of the four breath-test curve summary measures: cumulative PDR at 90 min, peak PDR, time to peak PDR, and time to recover 50% of the dose (cPDR-50). Best fit lines and correlation coefficients are given in Fig 5. Note that only those 11 breath curves that achieved 50% dose recovery within 5 hours were included in the correlation analysis of that cPDR-50. Parameter ρ , which controls the early phase of the curve, was most strongly correlated with the time to peak PDR ($R = -0.75$) and was moderately correlated with cumulative PDR recovered at 90 minutes ($R = 0.56$). No summary measure was strongly correlated with $\pi\rho$, the parameter that controls the late phase of the curve, and even the weak correlations were driven by one or two points. Parameter κ , the fraction of the dose that will be recovered, which acts as a vertical scaling parameter, was strongly correlated ($R = -0.78$) with time to recovering 50% of the dose; other correlations were weaker and driven by one or two points.

Discussion

Our work provides an alternative, mechanistic modeling approach to empirical curve fitting and summary measures when analyzing ¹³C substrate breath test curves. A three-parameter model—based on an underlying assumption

of substrate passage through an exponential, rate-limiting process; a gamma-distributed process; and a scaling factor representing the fraction of the tracer that would be recovered—can be fit to ¹³C breath curve data such that each parameter has a uniquely identifiable value. Although this work was illustrated using a ¹³C sucrose tracer, it is broadly applicable to most ¹³C substrate breath tests, since the metabolic pathways are broadly similar.

One important conclusion of our identifiability analysis is that a single breath test curve alone cannot necessarily resolve *all* the underlying metabolic processes that occur as part of substrate metabolism. Indeed, we found that a 3-parameter model with a simplifying assumption about the fast processes fit nearly all ¹³C-SBT curves as well as the full 6-parameter model. This result should be expected as the 3-parameter empirical models in Eqs (1) and (2) are typically flexible enough to capture breath test curve dynamics. This limitation of not being able to fully resolve the underlying transport and metabolism is not a limitation of the mechanistic approach and is instead a limitation inherent to the breath test itself: the breath test curve does not contain enough information on its own to support inference about all aspects of the metabolism, and, indeed, we should not expect it to. To further disaggregate key metabolic processes, other data—such as serial measurements of plasma ¹³C-bicarbonate or multiple breath tests repeated with different substrates on the same individual—would be required. On the other hand, if the goal is to translate characteristic curve dynamics into interpretable clinical information about an individual’s underlying health or disease state, our mechanistic approach ensures that the amount of information that can meaningfully be extracted from the breath curve is maximized.

Our approach also reveals some limitations of current practices for ¹³C substrate breath tests and offers approaches to mitigate and surmount them. Using our model-based approach to evaluate breath curves likely has advantages over conventional approaches, because model parameters, unlike conventional summary measures, have a mechanistic interpretation. Notably, summary measures, while attractive for their simplicity, appeared to be only somewhat correlated with the actual mechanistic rates underlying the breath curve. Some metabolic processes, including the rate-limiting step, appear to be poorly captured by all of the summary measures investigated. The summary measures such as cPDR at 90 min, peak PDR, and time to cPDR-50, were all associated with the scaling parameter κ , reflecting the fraction of the plasma bicarbonate excreted on the breath (as opposed to excreted in urine or sequestered). However, in most ¹³C breath test applications, this scaling factor is not the metabolic process of interest. The rate ρ was inversely correlated with time to peak PDR, and so this summary measure may be useful if the fast process is shown to be the process of interest. Even so, the model we presented here can be used to estimate these parameters directly, making breath curves more readily interpretable.

Our results also have implications for breath test administration. For instance, it may also be necessary to adjust the length of test duration depending on which underlying rate is of interest, e.g., longer tests may be needed to measure the limiting rate more accurately. By understanding the dynamics as a function of underlying metabolic rates, we can better design our testing procedures and our analysis plans.

Our work may need to be adjusted for other specific applications, which is why we presented the model reduction approach in full, so that it can be adapted for other applications as needed. One limitation of this analysis is that we assumed instantaneous gastric emptying because of the application of the small, liquid tracer. This work may need to be adapted to account for gastric emptying in the case of other tracer formats, e.g., when administered as part of a meal. To enhance the interpretation of breath test curves and develop a clinically meaningful diagnostic for the health of an underlying process, it will also be important to determine which aspects of the ¹³C metabolic pathway affect the mechanistic parameters we have identified here as capturing the breath test dynamics. This determination can be accomplished using multiple experiments designed to isolate different aspects of the metabolism. There is also a need to understand which aspects of the metabolism are folded into a single parameter and to characterize within-person (i.e., day-to-day) and between-person variation in these rates. This information would improve our ability to design breath tests to isolate specific aspects of the metabolism and to develop clinically meaningful thresholds for parameter values.

Conclusion

We developed a new approach to biological inferences from ¹³C breath test curves and connected specific aspects of curve dynamics to underlying biological rates. Better understanding how underlying biological processes impact different aspects of the breath curve enhances the clinical and research potential of the ¹³C-SBT, and other breath tests like it.

Acknowledgments. This project was funded through International Atomic Energy Agency coordinated research project E4.10.16. AB was supported by United States National Science Foundation (NSF) grant DMS1853032. GL was supported by United States National Institutes of Health (NIH) grant K01AI145080.

References

- [1] Braden B. Methods and functions: Breath tests. *Best Practice and Research: Clinical Gastroenterology*. 2009;23(3):337–352. <https://doi.org/10.1016/j.bpg.2009.02.014>.
- [2] Van Den Driessche M, Peeters K, Marien P, Ghooos Y, Devlieger H, Veereman-Wauters G. Gastric emptying in formula-fed and breast-fed infants measured with the ¹³C-octanoic acid breath test. *Journal of pediatric gastroenterology and nutrition*. 1999;29(1):46–51. <https://doi.org/10.1097/00005176-199907000-00013>.
- [3] Pelton N, Tivey D, Howarth G, Davidson G, Butler R. A novel breath test for the Non-invasive assessment of small intestinal mucosal injury following methotrexate administration in the rat. *Scandinavian Journal of Gastroenterology*. 2004;39(10):1015–1016. <https://doi.org/10.1080/00365520410003416>.
- [4] Ghooos YF, Maes BD, Geypens BJ, Mys G, Hiele MI, Rutgeerts PJ, et al. Measurement of gastric emptying rate of solids by means of a carbon-labeled octanoic acid breath test. *Gastroenterology*. 1993;104(6):1640–1647. [https://doi.org/10.1016/0016-5085\(93\)90640-X](https://doi.org/10.1016/0016-5085(93)90640-X).
- [5] Maes BD, Mys G, Geypens BJ, Evenepoel P, Ghooos YF, Rutgeerts PJ. Gastric emptying flow curves separated from carbon-labeled octanoic acid breath test results. *American Journal of Physiology - Gastrointestinal and Liver Physiology*. 1998;275(1 38-1):169–175. <https://doi.org/10.1152/ajpgi.1998.275.1.g169>.
- [6] Siegel J, Urbain J, Adler L, Charkes N, Maurer A, Krevsky B, et al. Biphasic nature of gastric emptying. *Gut*. 1988;29(1):85–89. <https://doi.org/10.1136/gut.29.1.85>.
- [7] Sanaka M, Yamamoto T, Nakayama S, Nagasawa K, Kuyama Y. Reliability of the time to maximal [¹³CO₂] excretion and the half-[¹³CO₂] excretion time as a gastric emptying parameter: Assessments using the Wagner-Nelson method. *Journal of Smooth Muscle Research*. 2007;43(5):201–209. <https://doi.org/10.1540/jsmr.43.201>.
- [8] Schillinger RJ, Mwakamui S, Mulenga C, Tembo M, Hodges P, Besa E, et al. ¹³C-sucrose breath test for the non-invasive assessment of environmental enteropathy in Zambian adults. *Frontiers in Medicine*. 2022;9. <https://doi.org/10.3389/fmed.2022.904339>.
- [9] Owino V, Ahmed T, Freemark M, Kelly P, Loy A, Manary M, et al. Environmental enteric dysfunction and growth failure/stunting in global child health. *Pediatrics*. 2016;138(6):e20160641. <https://doi.org/10.1542/>

[peds.2016-0641](#).

- [10] Crane RJ, Jones KD, Berkley JA. Environmental enteric dysfunction: an overview. *Food and Nutrition Bulletin*. 2015;36(1 Suppl):S76–S87. <https://doi.org/10.1177/15648265150361S113>.
- [11] WHO and UNICEF. Progress on drinking water, sanitation and hygiene: 2017 update and SDG baselines; 2017.
- [12] Ritchie BK, Brewster DR, Davidson GP, Tran CD, McNeil Y, Hawkes JS, et al. ¹³C-sucrose breath test: novel use of a noninvasive biomarker of environmental gut health. *Pediatrics*. 2009;124(2):620–626. <https://doi.org/10.1542/peds.2008-2257>.
- [13] Tran CD, Katsikeros R, Manton N, Krebs NF, Hambidge KM, Butler RN, et al. Zinc homeostasis and gut function in children with celiac disease. *The American Journal of Clinical Nutrition*. 2011;94(4):1026–1032. <https://doi.org/10.3945/ajcn.111.018093>.
- [14] Tran CD, Hawkes J, Graham RD, Kitchen JL, Symonds EL, Davidson GP, et al. Zinc-fortified oral rehydration solution improved intestinal permeability and small intestinal mucosal recovery. *Clinical Pediatrics*. 2015;54(7):676–682. <https://doi.org/10.1177/0009922814562665>.
- [15] Skovbjerg H, Sjöström H, Norén O. Purification and characterisation of amphiphilic lactase/phlorizin hydrolase from human small intestine. *European Journal of Biochemistry*. 1981;114(3):653–661. <https://doi.org/10.1111/j.1432-1033.1981.tb05193.x>.
- [16] Mones RL, Mercer GO. Ulcerative duodenitis in a child with celiac disease. *The Journal of Pediatrics*. 2011;158(5):857. <https://doi.org/10.1016/j.jpeds.2010.11.038>.
- [17] Slater C, Preston T, Weaver LT. Stable isotopes and the international system of units. *Rapid Communications in Mass Spectrometry*. 2001;15(15):1270–1273. <https://doi.org/10.1002/rcm.328>.
- [18] Shreeve W, Cerasi E, Luft R. Metabolism of [2-¹⁴C] pyruvate in normal, acromegalic and HGH-treated human subjects. *European Journal of Endocrinology*. 1970;65(1):155–169. <https://doi.org/10.1530/acta.0.0650155>.
- [19] Saccomani M, Bonadonna R, Cavegion E, DeFronzo RA, Cobelli C. Bicarbonate kinetics in humans: identification and validation of a three-compartment model. *American Journal of Physiology-Endocrinology And Metabolism*. 1995;269(1):E183–E192. <https://doi.org/10.1152/ajpendo.1995.269.1.e183>.

- [20] Bellman R, Åström KJJ. On structural identifiability. *Mathematical Biosciences*. 1970;7(3-4):329–339. [https://doi.org/10.1016/0025-5564\(70\)90132-X](https://doi.org/10.1016/0025-5564(70)90132-X).
- [21] Rothenberg TJ. Identification in Parametric Models. *Econometrica*. 1971;39(3):577–591. <https://doi.org/10.2307/1913267>.
- [22] Cobelli C, DiStefano JJ. Parameter and structural identifiability concepts and ambiguities: a critical review and analysis. *The American Journal of Physiology*. 1980;239(1):R7–24. <https://doi.org/10.1152/ajpregu.1980.239.1.R7>.
- [23] Raue A, Kreutz C, Maiwald T, Bachmann J, Schilling M, Klingmüller U, et al. Structural and practical identifiability analysis of partially observed dynamical models by exploiting the profile likelihood. *Bioinformatics*. 2009;25(15):1923–1929. <https://doi.org/10.1093/bioinformatics/btp358>.
- [24] Brouwer AF, Meza R, Eisenberg MC. Parameter estimation for multi-stage clonal expansion models from cancer incidence data: A practical identifiability analysis. *PLOS Computational Biology*. 2017;13(3):1–18. <https://doi.org/10.1371/journal.pcbi.1005431>.
- [25] Margaria G, Riccomagno E, Chappell MJ, Wynn HP. Differential algebra methods for the study of the structural identifiability of rational function state-space models in the biosciences. *Mathematical Biosciences*. 2001;174(1):1–26. [https://doi.org/10.1016/S0025-5564\(01\)00079-7](https://doi.org/10.1016/S0025-5564(01)00079-7).
- [26] Audoly S, Bellu G, D’Angiò L, Saccomani MP, Cobelli C. Global identifiability of nonlinear models of biological systems. *IEEE transactions on Bio-medical Engineering*. 2001 jan;48(1):55–65. <https://doi.org/10.1109/10.900248>.
- [27] Saccomani MP, Audoly S, D’Angiò L. Parameter identifiability of nonlinear systems: The role of initial conditions. *Automatica*. 2003;39(4):619–632. [https://doi.org/10.1016/S0005-1098\(02\)00302-3](https://doi.org/10.1016/S0005-1098(02)00302-3).
- [28] Eisenberg MC, Hayashi MAL. Determining identifiable parameter combinations using subset profiling. *Mathematical Biosciences*. 2014;256:116–126. <https://doi.org/10.1016/j.mbs.2014.08.008>. <https://arxiv.org/abs/1307.2298>.

Supplementary Files

This is a list of supplementary files associated with this preprint. Click to download.

- [Supportinginformation.pdf](#)
- [graphicalabstract.pdf](#)